Available online at BCREC website: https://bcrec.id

Bulletin of Chemical Reaction Engineering & Catalysis, 15 (2) 2020, 501-513

Research Article

Selective Reduction of Southeast Sulawesi Nickel Laterite using Palm Kernel Shell Charcoal: Kinetic Studies with Addition of Na_2SO_4 and NaCl as Additives

Achmad Shofi[1], Yayat Iman Supriyatna[2,*], Agus Budi Prasetyo[3]

[1]Public Works and Spatial Planning, Rembang Regency,Central Java, Indonesia.
[2]Research Unit for Mineral Technology, Indonesian Institute of Sciences, Lampung, Indonesia.
[3]Research Center for Metallurgy and Material, Indonesian Institute of Sciences, South Tangerang, Indonesia.

Received: 5th May 2020; Revised: 6th June 2020; Accepted: 12th June 2020;
Available online: 30th July 2020; Published regularly: August 2020

Abstract

The aim of the reduction process is to concentrate nickel at high temperatures with a certain carbonaceous material as a reducing agent. The use of chemicals like Na_2SO_4 and NaCl in the reduction process can increase the content and recovery of nickel in ferronickel concentrates. A selective reduction of laterite nickel was carried out in a non-isothermal and an isothermal using palm kernel shell charcoal as a reductant and with Na_2SO_4 and NaCl as additives. Firstly, the raw material is made into a pellet and dried in an oven at 100 °C for two hours. The pellets are weighed before and after the reduction process. The non-isothermal reduction process used the Thermal Gravimetric Analysis (TGA) method from a temperature of 100 to 1300 °C, with a heat rate of 10 °C per minute. The isothermal reduction at temperatures 500, 600, 700, 950, 1050, and 1150 °C occurred with a reduction time of 30, 60, and 90 minutes. The analysis is Inductively Coupled Plasma (ICP) to determine the content of nickel and iron from the reduction process, X-ray Diffraction (XRD) to see changes in the phases formed after the selective reduction process, and Scanning Electron Microscopy (SEM-EDX) for viewing the microstructure of the phase. The Differential Thermal Analyzer-Temperature Gravimetric Analysis (DTA-TGA) results show the endothermic at 256 °C, and the exothermic peak at 935 °C with a total mass loss of 42.15% at 1238 °C. The shrinking core model was used for the kinetic studies of the reduction process. The closest kinetic model to the experimental results is the Ginstling-Brounshtein model, with an activation energy value of 8.73 kcal/mol.

Keywords: additives; characterization; kinetic; nickel laterite; reductor; selective reduction

How to Cite: Shofi, A., Supriyatna, Y.I., Prasetyo, A.B. (2020). Selective Reduction of Southeast Sulawesi Nickel Laterite using Palm Kernel Shell Charcoal: Kinetic Studies with Addition of Na_2SO_4 and NaCl as Additives. *Bulletin of Chemical Reaction Engineering & Catalysis*, 15(2), 501-513 (doi:10.9767/bcrec.15.2.7733.501-513)

Permalink/DOI: https://doi.org/10.9767/bcrec.15.2.7733.501-513

1. Introduction

Nickel is now an essential metal in the world of infrastructure and technology, especially in the industries of stainless steel, Ni-based alloys, alloy steels, electroplating, and batteries. At present, more than 65% of nickel is used in the stainless-steel industry, and around 12% is used in the superalloy or nonferrous alloy manufacturing industry [1–4]. At this time, as much as 60% of the requirement of nickel is commercially supplied from sulfide rock. Around 70% of the

* Corresponding Author.
E-mail: yayat_iman@yahoo.com (Y.I. Supriyatna);
Telp: +62-721-350054, Fax: +62-721-350056

world's nickel reserves are trapped in the form of laterite in the saprolite and limonite layers [4,5]. Currently, the availability of nickel sulfide has decreased by only around 30% [6]. The increasing need for nickel and the depletion of sulfide rock reserves have forced the industry to consider laterite rock reserves as one of the primary sources of nickel [7]. Nickel laterite is not desirable as the primary source because of its relatively low nickel content. It requires more energy-intensive processing, sophisticated extraction methods, and is connected to higher greenhouse gas emissions compared to sulfide ore [3,8].

Indonesian nickel laterite contains around 1.45%, and so, conventional pyrometallurgical processes are ineffective [9]. The use of low-grade nickel ore as a raw material for the manufacture of ferronickel with content in concentrates > 4% Ni and recovery of high nickel metal has not been successful. The lack of success is caused by the lack of optimal methods and treatments during the selective reduction process, and so, it is necessary to study the right method in processing low-grade nickel ore into ferronickel concentrate.

Generally, the reducing agents used in reducing nickel laterite ore are coke, coal, or gas mixtures [10,11]. However, these reducing agents have several disadvantages when viewed in terms of ecology and their availability in nature. These are increasingly thinning out, hence it has become a challenge to find alternative energy sources that can replace the role of coke and coal in their function as reducing agents [12,13]. The use of palm kernel shell charcoal as a reducing agent in reducing nickel ore is an interesting one. The palm kernel shell is a waste of a natural resource (palm oil) and is currently not used optimally. The availability of palm oil land in Indonesia is increasingly becoming widespread; hence it can ensure the availability of palm kernel shells is abundance. Research related to the reduction of nickel laterite by using biomass as its reducing agent has been carried out by several researchers. Luo and Zhou [14], and Zuo *et al.* [15], in their research, have used biomass in the process of iron ore reduction. The effect of temperature reduction on the carbothermic reduction process of laterite ores using bio-coal as a reducing agent has been investigated by Chen *et al.* [16]. Another case, with research conducted by Foster *et al.* [17], entailed reducing nickel ore by using wood charcoal as its reducing agent. Despite several studies, no one has used palm kernel shell charcoal (PKS) as a reduction agent in reducing low-grade nickel ore.

The purpose of the reduction process is to concentrate nickel at high temperatures with some carbonaceous material as a reducing agent [18–21]. The use of chemicals like Na_2SO_4 and NaCl in the reduction process can increase the content and recovery of nickel in ferronickel concentrates. The reduction process is closely related to the reduction kinetics, in which kinetics is essential to know the time required for the reduction process and the controlling factors for the reduction reaction process. In kinetics, the reaction rate in a chemical reaction is studied. An analysis of the effect of various reaction conditions on the reaction rate provides information about the reaction mechanism and the transition state of a chemical reaction [22–26]. Therefore, in this paper, we present kinetic studies about a selective reduction of laterite nickel kinetic studies using palm shell charcoal as a reduction agent and the addition of Na_2SO_4 and NaCl as additives.

2. Materials and Methods

The ore samples were crushed to a size smaller than 149 μm and dried in an oven at a temperature of 105 °C for 24 hours to obtain a water content below 5%, before conducting the experiments. The process carried out in this research was a selective reduction of low-grade nickel ore at temperatures below 1200 °C by the addition of additives. Variations made were the reduction temperature and the reduction time. The raw material used was low-grade nickel laterite ore from Morombo Village in Konawe Utara Regency of Southeast Sulawesi Province.

2.1 Chemical Analysis

As the first step, some dry sample ore was used to analyze the chemical composition and concentration of the elements with XRF (X-Ray Fluorescence). The crystal structure and composition of mineral compositions were analyzed using XRD (X-Ray Diffraction). SEM-EDX (Scanning Electron Microscopy-Energy Dispersive X-ray Spectroscopy) was used to see the microstructure of the phase. The reducing agent used was palm kernel shell charcoal (PKSC) analyzed proximately. The next step is to weigh the ore resulting from the selective reduction process and then milling up to smaller than 74 μm using a vibrating sample mill and an analysis using ICP (Inductively Coupled Plasma) to determine the contents of nickel and iron from the reduction process. XRD was used to see the changes in the composition of

minerals or phases formed after the selective reduction process.

2.2 Thermo Gravimetric Analysis (TGA)

At the initial stage, a non-isothermal reduction test is carried out using DTA-TGA to determine the characterization of laterite ores during heat treatment. The TGA method deploys the principle of measuring mass loss during heat treatment. In contrast, DTA is a heat analysis technique in which the phase changes of material are measured as a function of temperature. In this study, the sample was heated from a temperature of 100 to 1300 °C with a heat rate of 10 °C per minute. The addition of a reductant is four stoichiometry without additives. The results of this experiment form the basis for experiments under isothermal conditions.

Adding one stoichiometry-reducing agent based on reaction numbers 1 to 7 follows [27]:

2 FeOOH	→	$Fe_2O_3 + H_2O$	(1)
3 Fe_2O_3 + CO	→	2 Fe_3O_4 + CO_2	(2)
Fe_3O_4 + CO	→	3 FeO + CO_2	(3)
FeO + CO	→	Fe + CO_2	(4)
NiO + CO	→	Ni + CO_2	(5)
Fe + Ni	→	FeNi	(6)
C + CO_2	→	2 CO	(7)

The additives added to the selective reduction process were Na_2SO_4 and NaCl, with a percentage of 10% by weight. The next stage is mixing the ore, reducing agent, and additives to make pellets. The function of adding additives is to increase the selectivity of Ni by reducing levels of unwanted components.

2.3 Reduction Test

The pellet was then dried in an oven at 100 °C for 2 hours. The reduction test was conducted at temperatures of 500, 600, 700, 950, 1050, and 1150 °C with a holding time of 30, 60, and 90 minutes. The pellets were weighed before and after the reduction process.

2.4 Data-fitting Model

The shrinking core model was applied to the data. For spherical particles, the slow step for the heterogeneous reaction represented by Eq. (8) can be (i) diffusion of gaseous reagent through the gas film layer on the particle surface, (ii) diffusion of fluid reagent through the blanket of ash to the surface of the unreacted particle, or (iii) reaction of the gaseous reagent with the unreacted particle surface [28].

A (fluid) + b B (solid) → solid product (8)

When the slow step is the chemical reaction with the unreacted particle surface, the conversion (α) as a function of time is described by Equation (9):

$$f(\alpha) = \frac{1}{k}\frac{d\alpha}{dt} = (1-\alpha)^n \quad (9)$$

$$\frac{d\alpha}{dt} = k(1-\alpha)^n \quad (10)$$

Assuming that the reduction process is perfect, the overall reaction is:

$$NiO_{(s)} + CO_{(g)} \rightarrow Ni_{(s)} + CO_{2\,(g)} \quad (11)$$

The value of α is the conversion (reduction reaction rate) with Equation (12):

$$\alpha_{Ni} = \frac{Ni_{RO} \times W_{RO}}{Ni_{ore} \times W_p} \quad (12)$$

where α is fraction that reacts, Ni_{RO} is reduced nickel content, W_{RO} is weight of the pellet after reduction, Ni_{ore} is nickel content in the ore, and W_p is weight of the pellet before reduction.

If a solid particle is assumed to have a spherical shape, with a volume of R where R is the radius of the ball. The equation that applies to this condition is:

$$1-(1-\alpha)^{1/3} = k_0 t \quad (13)$$

In this equation k_0 is a chemical constant obtained based on the following equation:

$$k_0 = \frac{bk'C}{\rho R} \quad (14)$$

where b is the stoichiometric coefficient of the reaction, C is the concentration of gas-phase reactant in the main body of gas, ρ is the molar density of the solid reactant, R is the radius of the particle, k is the chemical constant, and t is the time. When the slow step is the diffusion of reactant through the gas film layer on the particle surface, the conversion (α) as a function of time is described by Equation (15):

$$\alpha = k_d t \quad (15)$$

In this equation, k_d is a diffusional constant described by the following equation:

$$k_d = \frac{3bk_g C}{\rho R} \quad (16)$$

where b is the stoichiometric coefficient of the reaction, C is the concentration of a gas-phase reactant in the main body of the gas, ρ is the molar density of the solid reactant, R is the ra-

dius of the particle, k_g is the mass transfer coefficient between particle and fluid, and t is the time. Finally, when the resistance to diffusion through the ash controls the rate of reaction, the conversion (α) as a function of time is described by Equation (17):

$$1-\frac{2}{3}\alpha-(1-\alpha)^{2/3}=k_t t \quad (17)$$

Here, k_t is a diffusional constant given by the following equation:

$$k_t=\frac{3bD_eC}{\rho R^2} \quad (18)$$

where b is the stoichiometric reaction coefficient, C is the concentration of the fluid reagent in the bulk of the solution, ρ is the density of the solid reagent, R is the radius of the particle, D_e is the effective diffusion coefficient of the gaseous reactant in the ash layer, and t is the time.

3. Results and Discussions

3.1 Results of Analysis of Laterite Nickel Ore and Palm Kernel Shell Charcoal (PKSC)

Table 1 shows the XRF analysis results for laterite nickel ore. The test results show that nickel content is 1.4%, with a very high iron content (50.5% Fe) and low magnesium content. The nickel content indicates the nickel laterite ore used is nickel type low contents (limonite). The main characteristic of limonite ore is the presence of large amounts of Goethite (FeO.OH) or iron oxide hydrate minerals, nickel content between 0.5% and 1.7%, and iron content between 40 % and 60%. The non-metal impurities contained in the laterite nickel ore are 16.5% Si, 1.81% Mg, 0.177% Ca, and 4.86% Al. In limonite ore, a portion of nickel is associated in the goethite phase and a small portion of the lizardite phase.

The result of the XRD analysis in Figure 1 show that most of the iron is in the goethite phase, and most of the nickel substitutes the Fe atom in that phase, and a small number of other nickel is joined with Mg and Si in the form of olivine compounds. The undetectable mineral phase of nickel is possible because its concentration is below the detection limit. Other elements such as aluminum, silicon, calcium, and manganese, also associate to form Lizardite [$Mg_3(SiO_5)(OH)_4$] compounds. The combination of some nickel elements in the lizard-

Table 1. Results of XRF analysis of laterite nickel ore samples.

Element	Content (%wt)
Ni	1.40
Fe	50.50
Si	16.50
Mg	1.81
Al	4.86
Ca	0.17
Cr	2.68
Mn	0.84
Co	0.06

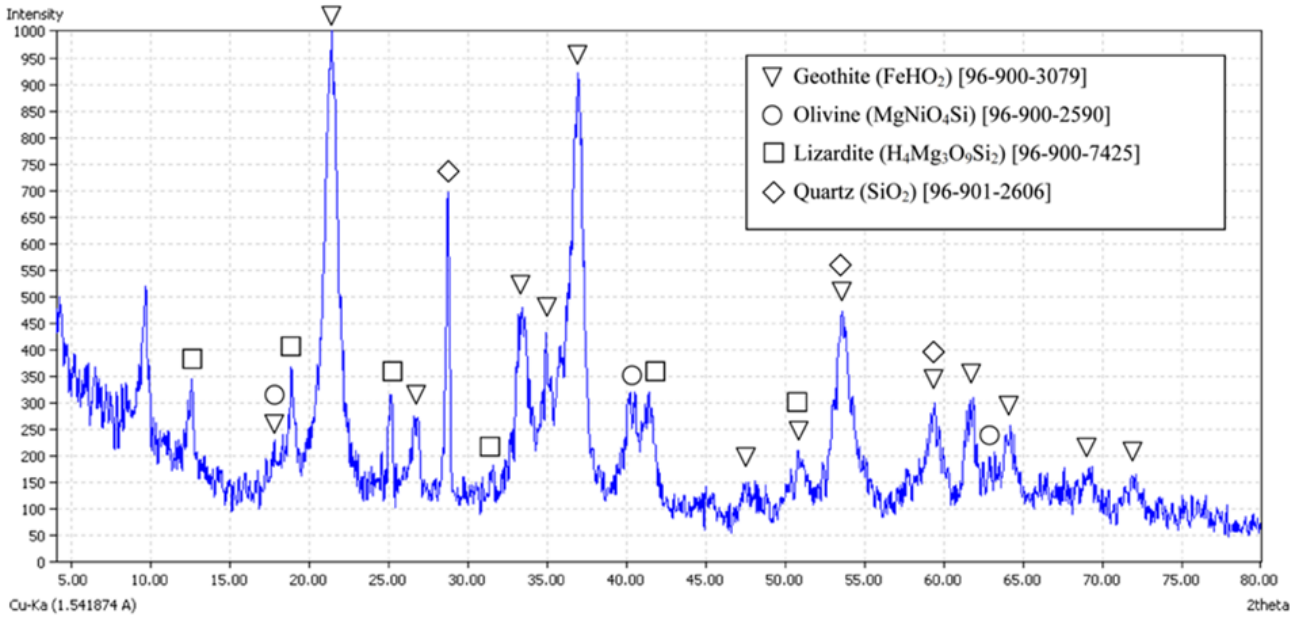

Figure 1. XRD analysis results of laterite nickel ore.

ite phase and others in the goethite crystal structure can be seen through SEM-EDS testing by seeing the mapping of the elements present in laterite nickel ore to determine the mineralogical structure of limonite ore as shown in Figure 2.

In Figure 2, it is seen that iron is spread almost all over the limonite ore along with oxygen. It can indicate that iron along with oxygen will form iron oxide in the form of either goethite or hematite. The nickel element, with its small size, is evenly distributed in almost all parts where most of the nickel element will be associated with the iron element in the crystal structure of goethite by substituting one of the iron atoms to (Fe,Ni)O(OH). In contrast, a small portion of the nickel element will be substituted with magnesium and silica to form olivine compounds. That can occur because nickel and magnesium have almost the same radius and ion charge. Mg and Si bind together with oxygen and form the lizardite phase [$Mg_3(Si_2O_5)(OH)_4$]. While silicon binds with oxygen to form silica (SiO_2), these results are entirely consistent with qualitative analysis using XRD.

The result of the proximate analysis in Table 2 show a high carbon content in PKSC so that it is good to be used as a reducing agent. However, one aspect to be considered is that the ash content is quite high. This ash is mainly SiO_2, which will become an impurity in the reduction process.

Table 2. Results of the PKS charcoal proximate analysis used (base: ADB).

No	Proximate Analysis	PKSC
1	FC (%)	77.00
2	VM (%)	22.57
3	Ash (%)	21.00
4	Moisture (%)	0.43

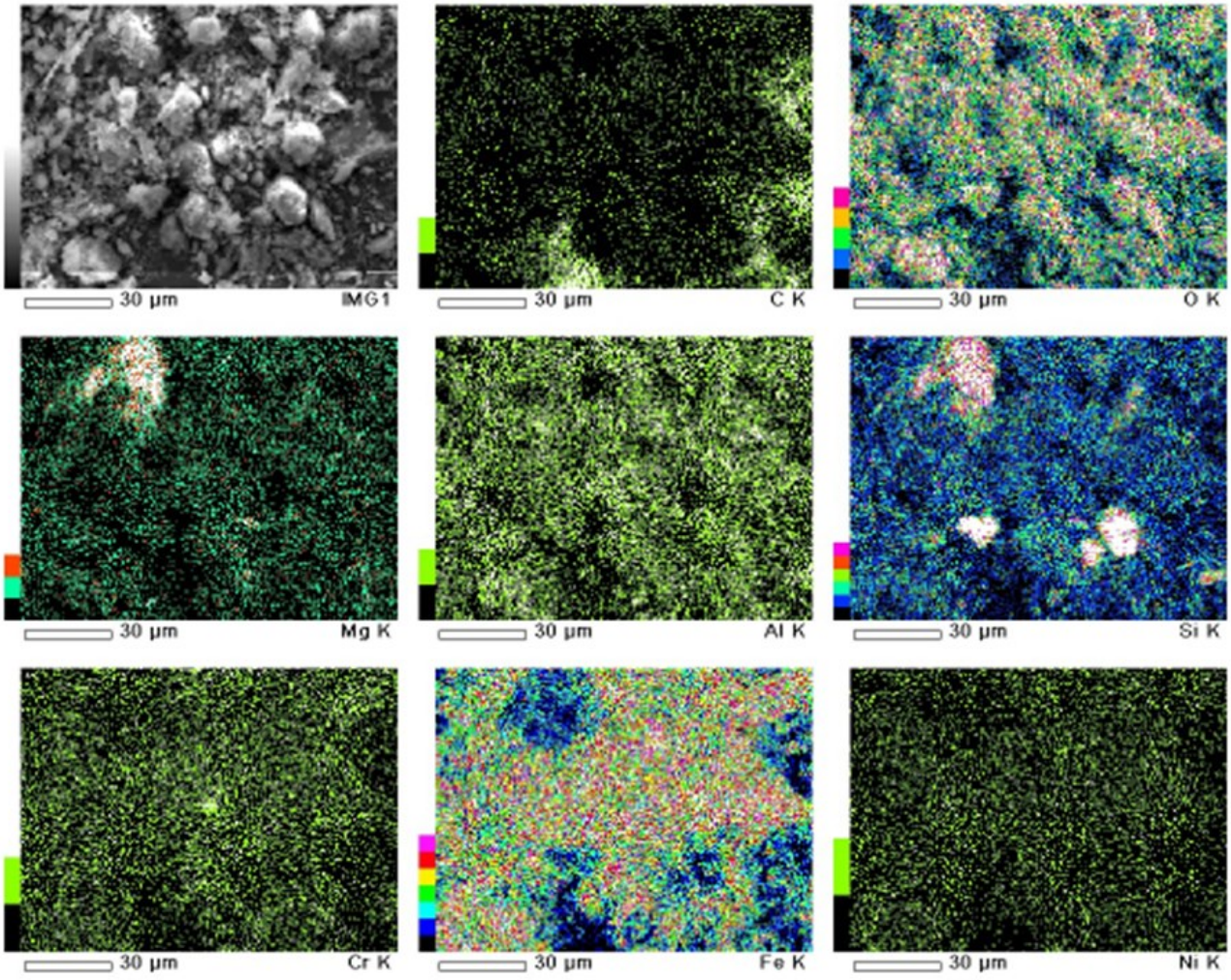

Figure 2. Photograph of the results of element mapping on laterite nickel ore.

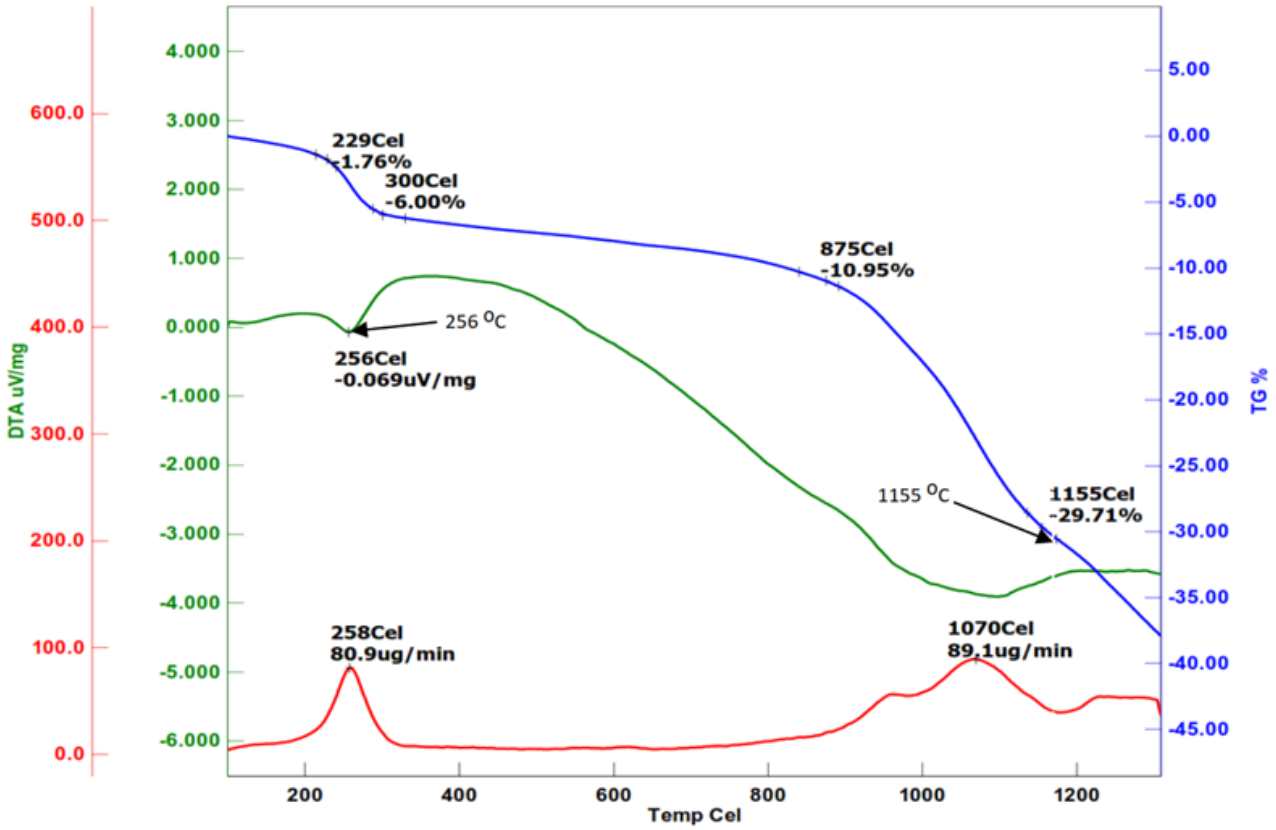

Figure 3. DTA-TGA curve of low-grade nickel ore + PKSC.

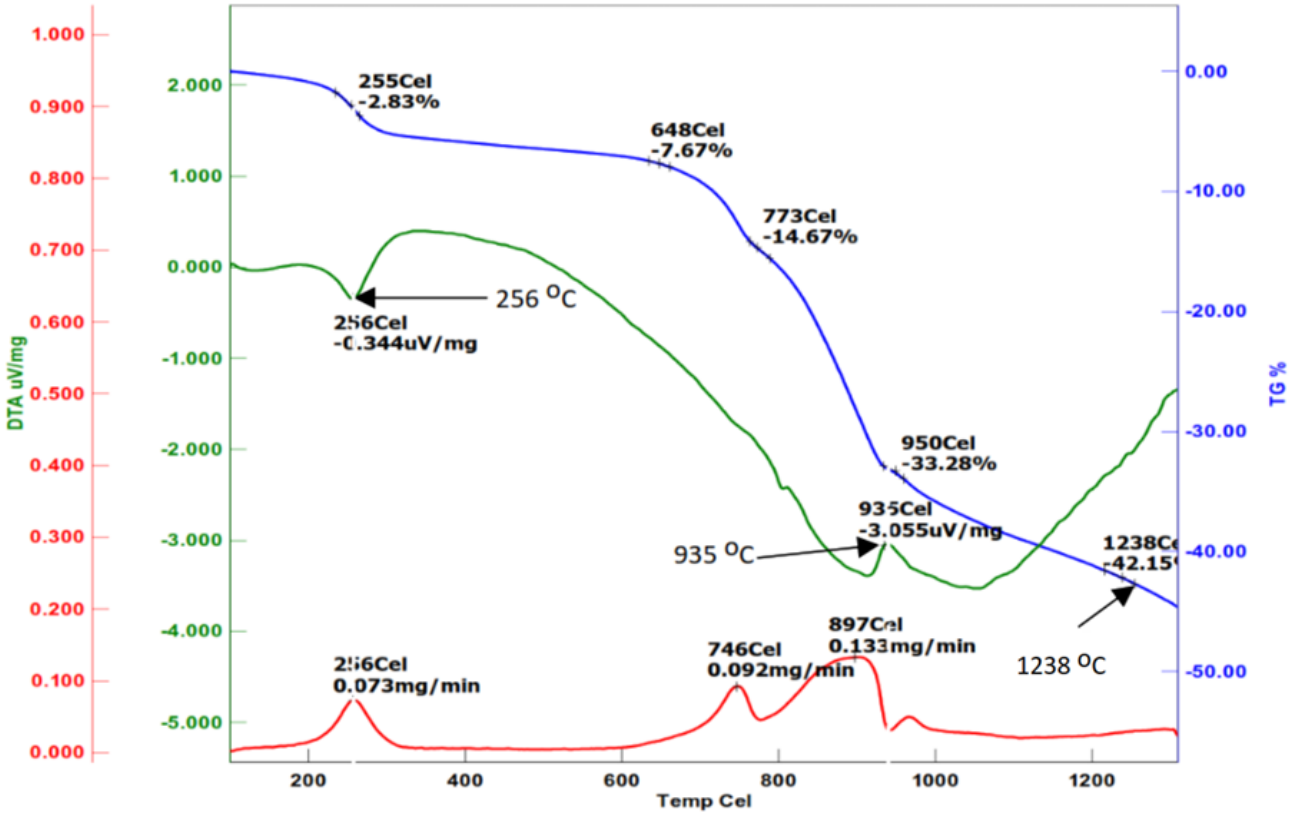

Figure 4. DTA-TGA curve of low-grade nickel ore + PKSC + additive.

3.2 Non-Isothermal Reduction

The results of the reduction test in non-isothermal conditions are shown in the form of the TDA-TGA curve in Figure 3 and Figure 4. Figure 3 shows that the endothermic peak occurs only at 256 °C, while the exothermic peak does not appear on the graph with a total mass loss of 29.71% at a temperature of 1155 °C. Even though the peak is not visible, a surface water evaporation reaction occurs at a temperature of 105 °C. An endothermic peak occurs at a temperature of 256 °C, which begins with a mass loss of 4.24% from a temperature of 229 to 300 °C. This indicates a change in thermal stability, namely the process of dehydroxylation of goethite [FeO(OH)] minerals that are transformed into hematite (Fe_2O_3) [29,30]. The decomposition temperature, which tends to be lower than the results of other studies around 300 °C, is due to the low crystallinity of the goethite structure [29].

However, the decomposition of goethite into hematite crystals occurs at 900 °C [21,31]. From a temperature of 300 to 875 °C, a mass reduction of 4.95% was detected, which means that there was a reduction in iron and nickel oxide as well as the presence of gasification from carbon (1.4% Ni). At a temperature interval of 875 to 1155 °C, there was a significant mass loss of 18.76%, which caused further metal oxide reduction so that oxygen and carbon were lost from the system. The temperature of the third endothermic reaction at 1070 °C indicates the dehydroxylation reaction of the lizardite phase to olivine or recrystallization from the fayalite phase (Fe_2SiO_4) [32].

Figure 4 is a TGA-DTA test curve of low-grade nickel samples with four stoichiometric reducers and the additives Na_2SO_4 and NaCl; each account for 10% of the weight of the test sample. The curve shows an endothermic peak at 256 °C, and there is an exothermic peak at 935 °C with a total mass loss of 42.15% at 1238 °C. The first endothermic reaction is the surface water evaporation reaction at a temperature of 105 °C, but is not detected. The endothermic peak at a temperature of 256 °C is a dehydroxylation process of goethite [FeO(OH)] minerals that are transformed into hematite (Fe_2O_3) with a mass reduction of 2.83% at a temperature of 255 °C. At a temperature interval of 255 to 648 °C, a mass loss of 4.84% occurred because of the formation of sulfur gas, sulfidation reactions of metal oxides, nickel chlorination, and loss of water crystals in lizardite even in small amounts. At a temperature interval of 648 to 950 °C there was a significant mass reduction of 25.61% due to the continued reduction of nickel and iron oxide to metals, dehydroxylation of the lizardite phase [$(Mg,Fe)_3Si_2O_5(OH)_4$] which lost its water crystals to olivine ($(Mg,Fe)_2SiO_4$) [4,33], reduction of nickel and iron oxide to metals, decomposition of metal sulfides such as troilite, and loss of sulfur in the system [30]. It is possible to refer the fourth endothermic reaction occurring in the temperature range of 900 °C to the perfect reduction of goethite to magnetic, changes in the magnetic properties of hematite, and formation of wustite from magnetic. The exothermic peak at 935 °C indicates the solidification reaction of the components forming the Fe-FeS liquid phase system.

3.3 Nickel Reduction Rate

The relationship between the reduction rate and the reduction time to the temperature obtained are respectively shown in Figure 5 and Figure 6, respectively.

Figure 5 shows that the reduction rate of nickel pellets did not change significantly with an increase in the reduction time, especially

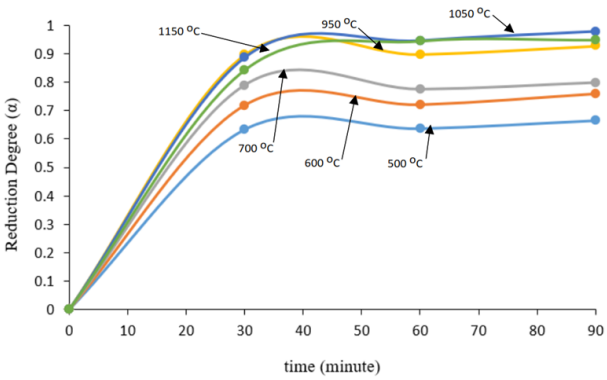

Figure 5. The reduction degree vs. time at several reduction temperatures.

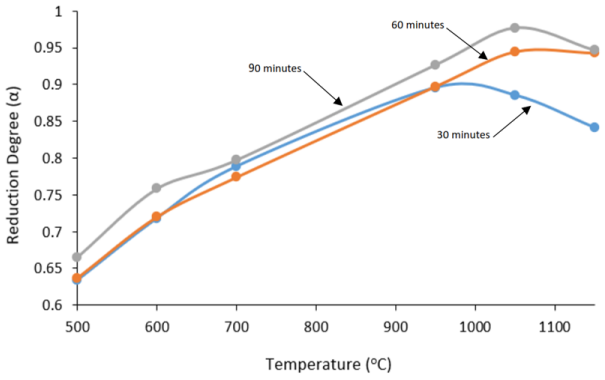

Figure 6. The reduction degree vs. temperature at some reduction time.

between 30 and 90 minutes. Significantly, an increase in the rate of reduction reaction is seen from 0 to 30 minutes. It shows that the reduction rate is divided into two stages, viz. the first stage of the reduction rate goes very fast (0 – 30 minutes), and then the reduction rate slows down after the reduction time of 30 minutes. In the first step, the reaction reduction that occurs is the process of reducing carbon and nickel oxide because CO gas is still minimal. In the next step (after 30 minutes), because of the increased metal products, the carbon as a reducing agent cannot contact the nickel oxide; hence the CO gas, which has the role of replacing carbon as a reducing agent. Meanwhile Figure 6 shows the increase in temperature has a very significant effect on the rate of reduction of nickel pellets. The results showed a significant increase from 500 to 1100 °C, whereas, after 1100 °C, the temperature decreased.

3.4 Reduction Kinetic Model

Kinetic models based on this research use fitting models. The model used is shown in Table 3. Table 4 shows the data of the constants of the reduction reaction rate. Table 4 is obtained from the linear equation (Figure 7) obtained for each temperature of the experiment at some reduction times. In the linear equation, the resulting slope is the value of k (rate constant).

To find out the activation energy in the kinetics of the nickel reduction process by using the extraction-reduction percentage parameter between variations in temperature and reduction holding time, we can use the Arrhenius equation, as in Equation (20), which is a derivative in Equation (19).

$$k = Ae^{-\frac{Ea}{RT}} \tag{19}$$

$$-\ln k = -\ln A + \frac{Ea}{RT} \tag{20}$$

Table 3. Equation of the kinetic model.

Model	Reaction Mechanism	Integral $g(\alpha)$
R2	Contracting area	$1-(1-\alpha)^{1/2}$
R3	Contracting volume	$1-(1-\alpha)^{1/3}$
D3	3-D diffusion (Jander)	$\left[1-(1-\alpha)^{1/3}\right]^2$
D4	3-D diffusion (Ginstling-Brounshtein)	$1-\frac{2}{3}\alpha-(1-\alpha)^{2/3}$
A2	2-D growth of nuclei (Avrami-Erofeev Equation)	$\left[-\ln(1-\alpha)\right]^{1/2}$
A3	3-D growth of nuclei (Avrami-Erofeev Equation)	$\left[-\ln(1-\alpha)\right]^{2/3}$

Table 4. The results of the calculation of the rate of reduction of the experimental reaction constants following the model.

T (°C)	k (minutes^{-1})					
	Contracting area	Contracting volume	Jander	Ginstling-Brounshtein	Avrami-Erofeev 2D	Avrami Erofeev 3D
500	0.0004	0.0003	0.0002	0.0001	0.0007	0.0010
600	0.0007	0.0005	0.0004	0.0003	0.0011	0.0015
700	0.0002	0.0001	0.0001	0.0001	0.0003	0.0004
950	0.0009	0.0009	0.0010	0.0004	0.0019	0.0029
1050	0.0031	0.0034	0.4410	0.0016	0.0078	0.0125
1150	0.0028	0.0027	0.0030	0.0013	0.0059	0.0091

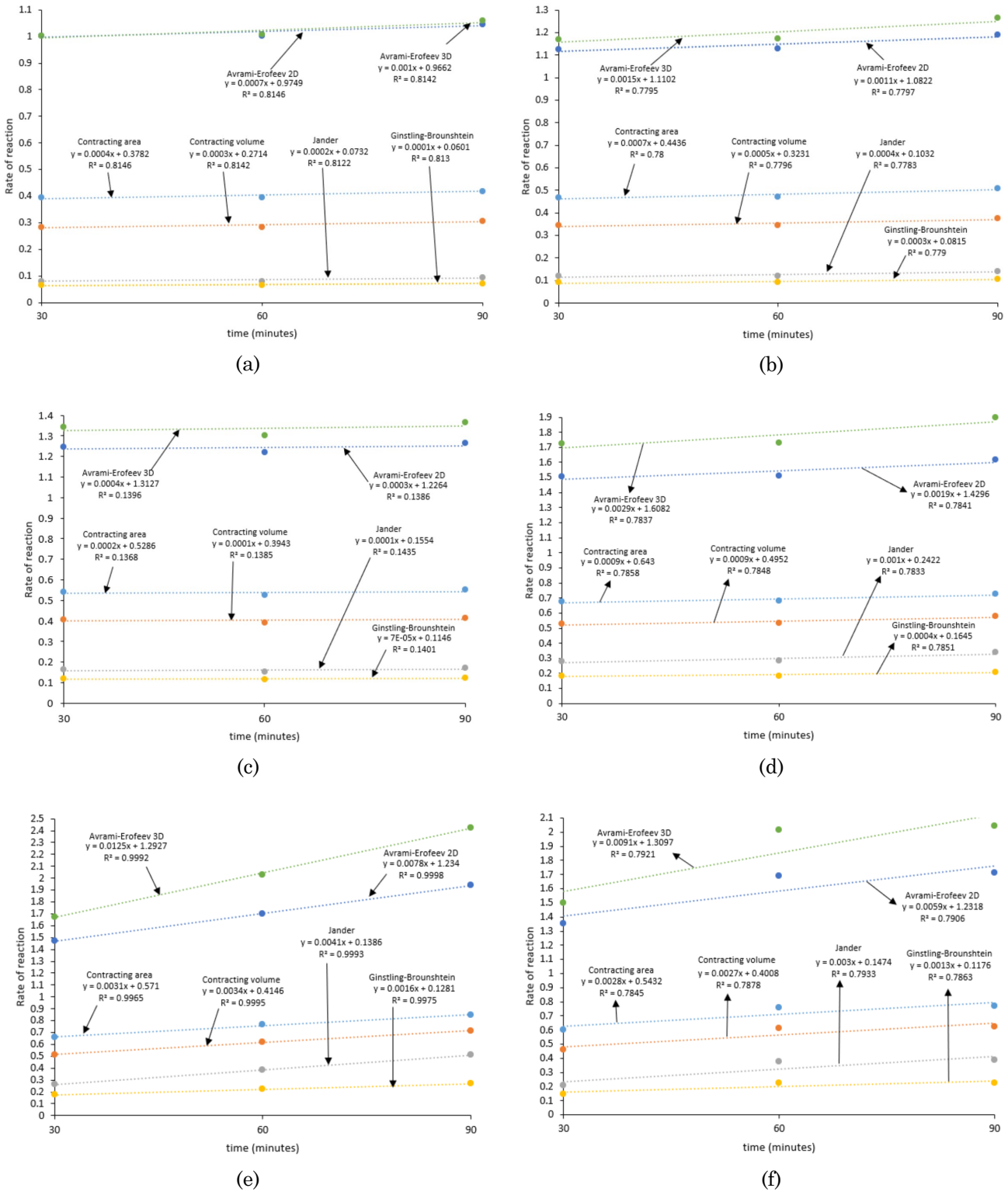

Figure 7. Graph of the relationship of the reaction rate to the reduction time at several reduction temperatures for several models; (a) T = 500 °C, (b) T = 600 °C, (c) T = 700 °C, (d) T = 950 °C, (e) T = 1050 °C; (f) T = 1150 °C).

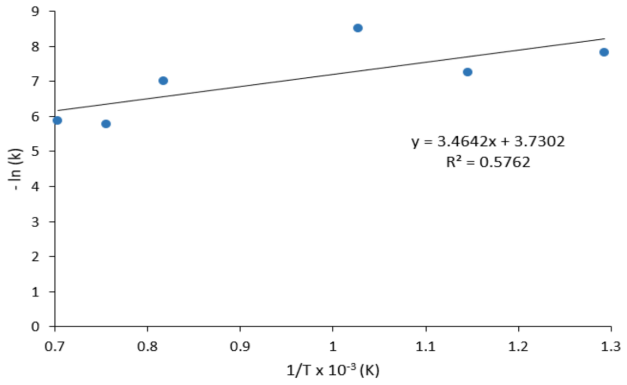

(a) Contracting area model

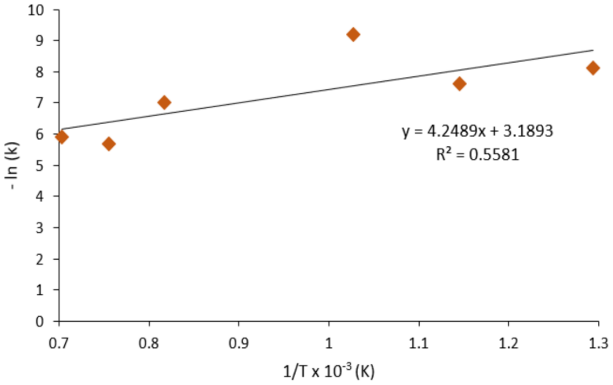

(b) Contracting volume model

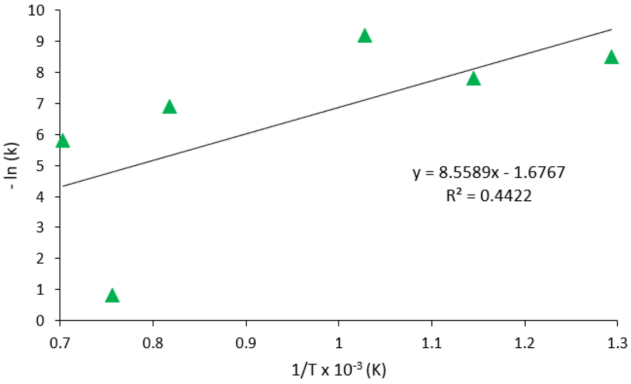

(c) Jander

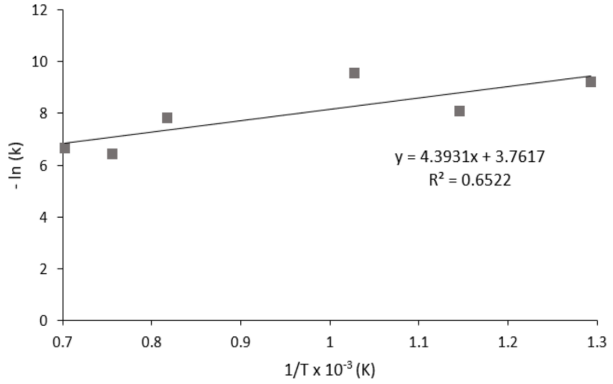

(d) Ginstling-Brounshtein

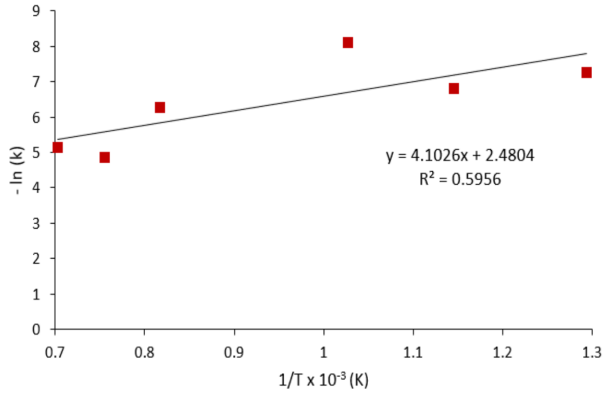

(e) Avrami-Erofeev 2D

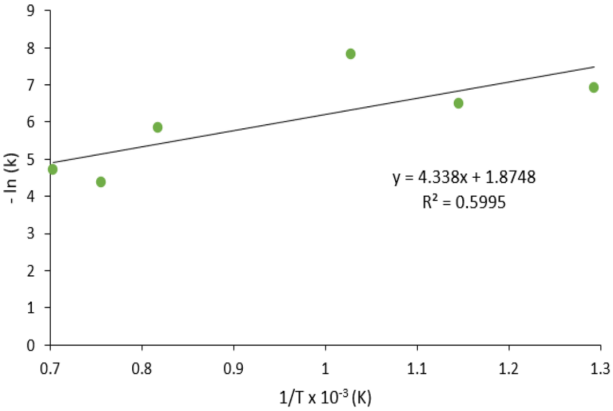

(f) Avrami-Erofeev 3D

Figure 8. Graph of the relationship of 1/T×10³ (K) to –ln *k* for each model.

The theory shows the comparison and effect of temperature on the reaction rate constant through a graph plot $1/T$ to $-\ln k$. Table 5 shows the calculated data based on the reaction rate constant to temperature, and Figure 8 is the graph of the relationship $1/T$ to $-\ln k$.

Based on Table 5 and Figure 8, the regression equation for each model is known if it is correlated with the Arrhenius equation. In Figure 8, the amount of activation energy is determined through a regression made from the results of the graph plot. with the ideal gas constant (R) = 1.987 cal/mol.K so the activation energy (Ea) obtained is the product of the ideal gas constant with the value of Ea/R. The complete results of the activation energy calculation based on the kinetic model are shown in Table 6. The activation energy shows the minimum energy for the reaction to occur. At the reaction rate controlled by gas diffusion, requires activation energy of 1–3 kcal/mol, if the reaction rate is controlled by a mixture of chemical reactions and gas diffusion requires energy of 5-8 kcal/mol, and the rate controlled by chemical reaction requires the energy of more than 10 kcal/mol [34]. Based on the linear regression results, the five models used have a coefficient of determination (R^2) that has still not reached the value $R^2 = 1$. The value of this correlation coefficient indicates the suitability of the model used to describe the reduction kinetics process. Closer to the value of $R^2 = 1$, then the model is used more precisely to describe the kinetics of the reduction taking place. The coefficient of determination closest to the value of $R^2 = 1$ of the five models used is the coefficient of determination obtained from the Ginstling-Brounshtein model. The result of the calculation for the activation energy value, according to this model, is 8.73 kcal/mol. Based on the value of this activation energy, the step that controls the reduction kinetics can be categorized as a mixture of chemical reactions and gas diffusion.

4. Conclusions

Nickel laterite contents in this study are 1.4% with a very high iron content of 50.5% and low magnesium. The non-metal impurities contained in the laterite nickel ore are 16.5% Si, 1.81% Mg, 0.177% Ca, and 4.86% Al. The XRD results show that most of the iron is in the goethite phase, and most of the nickel substitutes the Fe atom. Other elements such as aluminum, silicon, calcium, and manganese will also associate to form Lizardite [$Mg_3(SiO_5)(OH)_4$] compounds. The DTA-TGA results show the endothermic at 256 ºC, and the exothermic peak at 935 ºC with a total mass loss of 42.15% at 1238 ºC. The reduction rate is divided into two stages. The first stage of the reduction rate goes very fast (0 – 30 minutes), and then the reduction rate slows down after 30 minutes. The increase in temperature has a significant effect on the reduction rate of nickel pellets, with a significant increase from 500 °C to 1100 °C. The shrinking core model was used for the kinetic studies of the reduction process. The coefficient of determination closest to the value of $R^2=1$ of the five models used is obtained from the Ginstling-Brounshtein model with an activation energy value of 8.73 kcal/mol. Based on the value of this activation energy, the step that controls the reduction kinetics is a mixture of chemical reactions and gas diffusion.

Table 6. *Ea* calculation results for the various models used.

Model	Activation energy (kcal/mol)
Contracting area	6.88
Contracting volume	8.44
Jander	17.01
Ginstling-Brounshtein	8.73
Avrami-Erofeev 2D	8.15
Avrami-Erofeev 3D	8.62

Table 5. The calculation results of the reduction temperature to the reaction rate constant.

1/T	$-\ln k$					
	Contracting area	Contracting volume	Jander	Ginstling-Brounshtein	Avrami-Erofeev 2D	Avrami Erofeev 3D
0.001293	7.82	8.111	8.52	9.21	7.26	6.91
0.001145	7.26	7.601	7.822	8.11	6.81	6.50
0.001028	8.52	9.211	9.212	9.57	8.11	7.82
0.000818	7.01	7.011	6.91	7.82	6.26	5.84
0.000756	5.77	5.681	0.82	6.44	4.85	4.38
0.000703	5.88	5.911	5.81	6.64	5.13	4.69

Acknowledgments

We wish to thank the Research Unit for Mineral Technology-Indonesian Institute of Sciences (BPTM-LIPI) and those who have supported this research.

Authors Contributions

Achmad Shofi has carried out the characterization and study of the selective reduction, Yayat Iman Supriyatna has analyzed data and written the manuscript, and Agus Budi Prasetyo has helped analyze the sample and product.

References

[1] Barkas, J. (2010). Drivers and Risks for Nickel Demand 7th China Nickel Conference. Shanghai.

[2] Li, Y., Sun, Y., Han, Y., Gao, P. (2013). Coal-based reduction mechanism of low-grade laterite ore. *Transactions of Nonferrous Metals Society of China*, 23(11), 3428–3433. DOI: 10.1016/S1003-6326(13)62884-8

[3] Mudd, G.M. (2010). Global trends and environmental issues in nickel mining : Sulfides versus laterites. *Ore Geology Reviews*, 38(1–2), 9–26. DOI:10.1016/j.oregeorev.2010.05.003

[4] Kim, J., Dodbiba, G., Tanno, H., Okaya, K., Matsuo, S., Fujita, T. (2010). Calcination of low-grade laterite for concentration of Ni by magnetic separation. *Minerals Engineering*, 23(4), 282–288. DOI: 10.1016/j.mineng.2010.01.005

[5] Supriyatna, Y.I., Sihotang, I.H., Sudibyo, S. (2019). Preliminary Study of Smelting of Indonesian Nickel Laterite Ore using an Electric Arc Furnace. *Materials Today: Proceedings*, 13, 127–131. DOI: 10.1016/j.matpr.2019.03.201

[6] Agatzini-Leonardou, S., Tsakiridis, P.E., Oustadakis, P., Karidakis, T., Katsiapi, A. (2009). Hydrometallurgical process for the separation and recovery of nickel from sulphate heap leach liquor of nickeliferrous laterite ores. *Minerals Engineering*, 22(14), 1181–1192. DOI: 10.1016/j.mineng.2009.06.006

[7] Pickles, C.A. (2004). Microwave heating behaviour of nickeliferous limonitic laterite ores. *Mineral Engineering*, 17, 775–784. DOI: 10.1016/j.mineng.2004.01.007

[8] Kyle, J. (2010). Nickel laterite processing technologies – where to next. *ALTA 2010 Nickel/Cobalt/Copper Conference*, 1–33. Perth, Western Australia: Murdoch Research Repository.

[9] Norgate, T., Jahanshahi, S. (2011). Assessing the energy and greenhouse gas footprints of nickel laterite processing. *Minerals Engineering*, *24*(7), 698–707. DOI: 10.1016/j.mineng.2010.10.002

[10] Li, B., Ding, Z., Wei, Y., Wang, H., Yang, Y., Barati, M. (2018). Kinetics of Reduction of Low-Grade Nickel Laterite Ore Using Carbon Monoxide. *Metallurgical and Materials Transactions B*, 49(6), 3067–3073. DOI: 10.1007/s11663-018-1367-8

[11] Song, C., Shu-qiang, G., Yu-ling, X., Lan, J., Wei-zhong, D. (2014). Research on Selective Reduction of Laterite Nickel Ore by CO_2/H_2 Mixed Gas. *Advanced Materials Research*, 1025–1026, 814–819. DOI: 10.4028/www.scientific.net/AMR.1025-1026.814

[12] Sihotang, I.H., Supriyatna, Y.I., Ismail, I., Sulistijono, S. (2018). The effect of smelting time and composition of palm kernel shell charcoal reductant toward extractive Pomalaa nickel laterite ore in mini electric arc furnace. *AIP Conference Proceedings*, 1945(1), 020023. DOI: 10.1063/1.5030245

[13] Supriyatna, Y.I., Zulhan, Z., Triapriani, Y. (2018). The ferromanganese production using Indonesian low-grade manganese ore using charcoal and palm kernel shell as reductant in mini electric arc furnace. *IOP Conference Series: Materials Science and Engineering,* 285, 012022, DOI: 10.1088/1757-899X/285/1/012022

[14] Luo, S., Yi, C., Zhou, Y. (2011). Direct reduction of mixed biomass-Fe_2O_3 briquettes using biomass-generated syngas. *Renewable Energy*, 36(12), 3332–3336. DOI: 10.1016/j.renene.2011.05.006

[15] Zuo, H., Hu, Z., Zhang, J., Li, J., Liu, Z. (2013). Direct reduction of iron ore by biomass char. *International Journal of Minerals, Metallurgy and Materials*, 20(6), 514–521. DOI: 10.1007/s12613-013-0759-7

[16] Chen, G., Hwang, W., Liu, S., Shiau, J., Chen, I. (2014). Effect of Reduction Temperature On The Carbothermic Reduction Process Of Laterite Ores Mixing With Bio-Coal. *Metal,* 56 (4), 550-555. DOI: 10.2320/matertrans.M2014315.

[17] Forster, J., Pickles, C.A., Elliott, R. (2015). Microwave carbothermic reduction roasting of a low grade nickeliferous silicate laterite ore. *Mineral Engineering*, 88, 18-27, DOI: 10.1016/j.mineng.2015.09.005

[18] Chen, J., Hayes, P.C. (2019). Mechanisms and Kinetics of Reduction of Solid NiO in CO/CO_2 and CO/Ar Gas Mixtures. *Metallurgical and Materials Transactions B*, 50(6), 2623–2635. DOI: 10.1007/s11663-019-01662-5

[19] Manukyan, K.V., Avetisyan, A.G., Shuck, C.E., Chatilyan, H.A., Rouvimov, S., Kharatyan, S.L., Mukasyan, A.S. (2015). Nickel Oxide Reduction by Hydrogen: Kinetics and Structural Transformations. *Journal of Physical Chemistry C*, 119(28), 16131–16138. DOI: 10.1021/acs.jpcc.5b04313

[20] Qu, G., Zhou, S., Wang, H., Li, B., Wei, Y. (2019). Production of Ferronickel Concentrate from Low-Grade Nickel Laterite Ore by Non-Melting Reduction Magnetic Separation Process. *Metals*, 9(1340), 1–11. DOI: 10.3390/met9121340

[21] Rodrigues, F., Pickles, C. A., Peacey, J., Elliott, R., Forster, J. (2017). Factors Affecting the Upgrading of a Nickeliferous Thermal Growth and Magnetic Separation. *Minerals*, 7(176), 1–21. DOI: 10.3390/min7090176

[22] Dong, J., Wei, Y., Zhou, S., Li, B., Yang, Y., Mclean, A. (2018). The Effect of Additives on Extraction of Ni, Fe and Co from Nickel Laterite Ores. *Journal of The Minerals, Metals & Society*, 70(10), 2365–2377. DOI: 10.1007/s11837-018-3032-8

[23] Jiang, M., Sun, T., Liu, Z., Kou, J., Liu, N., Zhang, S. (2013). Mechanism of sodium sulfate in promoting selective reduction of nickel laterite ore during reduction roasting process. *International Journal of Mineral Processing*, 123, 32–38. DOI: 10.1016/j.minpro.2013.04.005

[24] Rao, M., Li, G., Zhang, X., Luo, J., Peng, Z., Jiang, T. (2016). Reductive Roasting of Nickel Laterite Ore with Sodium Sulfate for Fe-Ni Production. Part I: Reduction/Sulfidation Characteristics. *Separation Science and Technology*, 51 (8), 1408-1420. DOI: 10.1080/01496395.2016.1162173

[25] Yang, S., Du, W., Shi, P., Shangguan, J., Liu, S., Zhou, C., Chen, P., Fan, H. (2016). Mechanistic and Kinetic Analysis of Na2SO4 - Modified Laterite Decomposition by Thermogravimetry Coupled with Mass Spectrometry. *PLOS ONE*, 11(6), 1–21. DOI: 10.1371/journal.pone.0157369

[26] Zhou, S., Wei, Y., Li, B., Wang, H., Ma, B., Wang, C. (2016). Mechanism of Sodium Chloride in Promoting Reduction of High-Magnesium Low-Nickel Oxide Ore. *Scientific Reports*, 6, 1–12. DOI: 10.1038/srep29061

[27] Zevgolis, E., Zografidis, C., Halikia, I. (2010). The reducibility of the Greek nickeliferous laterites : a review. *Mineral Processing and Extractive Metallurgy*, 119(1), 9–18. DOI: 10.1179/174328509X431472

[28] Levenspiel, O. (1999). Chemical Reaction Engineering. In *Chemical Reaction Engineering Third Edition* (pp. 566–586).

[29] Connor, F.O., Cheung, W.H., Valix, M. (2006). Reduction roasting of limonite ores : effect of dehydroxylation. *International Journal of Mineral Processing*, 80, 88–99. DOI: 10.1016/j.minpro.2004.05.003

[30] Elliott, R., Rodrigues, F., Pickles, C.A., Peacey, J., De, L. (2015). A two-stage thermal upgrading process for nickeliferous limonitic laterite ores. *Canadian Metallurgical Quarterly*, 54 (4), 395–405. DOI: 10.1179/1879139515Y.0000000009

[31] Elliott, R., Pickles, C.A., Forster, J. (2016). Thermodynamics of the Reduction Roasting of Nickeliferous Laterite Ores. *Journal of Minerals and Materials Characterization and Engineering*, 4, 320–346. DOI: 10.4236/jmmce.2016.46028

[32] Donghua, H., Jianliang, Z., Rui, M.A.O., Mingming, C.A.O. (2011). Thermal behaviors and growth of reduced ferronickel particles in carbon-laterite composites. *Rare Metals*, 30(6), 681–687. DOI: 10.1007/s12598-011-0449-4

[33] Li, B., Wang, H., Wei, Y. (2011). The reduction of nickel from low-grade nickel laterite ore using a solid-state deoxidisation method. Mineral Engineering, 24, 1556–1562. DOI: 10.1016/j.mineng.2011.08.006

[34] Habashi, F. (1997). Handbook of Extractive Metallurgy Volume II : Primary Metals, Secondary Metals, Light Metals. New York: WILEY-VCH.